Dalton Transactions

Electrostatic Polarization of Nonpolar Substrates: A Study of Interactions Between Simple Cations and Mo-bound N_2

Journal:	*Dalton Transactions*
Manuscript ID	DT-ART-04-2019-001606.R1
Article Type:	Paper
Date Submitted by the Author:	24-May-2019
Complete List of Authors:	Pap, Levente; University of Wyoming, Department of Chemistry Couldridge, Adam; University of Wyoming, Department of Chemistry Arulsamy, Navamoney; Univ of Wyoming, Chemistry Hulley, Elliott; University of Wyoming, Department of Chemistry

Dalton Transactions

ARTICLE

Electrostatic Polarization of Nonpolar Substrates: A Study of Interactions Between Simple Cations and Mo-bound N_2

Levente G. Pap,[a] Adam Couldridge,[a] Navamoney Arulsamy,[a] Elliott Hulley[a†]

Received 00th January 20xx,
Accepted 00th January 20xx

DOI: 10.1039/x0xx00000x

www.rsc.org/

Although a great deal of catalytic studies have focused on covalent interactions between substrates and catalyst centers, recognition of the importance of noncovalent and ionic interactions is driving new approaches to catalyst design. Electrostatic interactions with simple cations (those with little covalency, such as alkali metals) play crucial roles in many catalytic processes, but these effects are challenging to study due to their complicated solvation and speciation behaviour. These effects are particularly difficult to study during cation-mediated reactions with weakly-polar or non-polar substrates. Dinitrogen is one of the most nonpolar substrates known to be affected by electrostatic interactions in both heterogeneous and homogeneous reactions but understanding the significance of these effects requires further exploration. To examine these effects systematically, a new multidentate ligand framework bearing pendent crown ethers has been developed and incorporated into a series of Mo(0)-based dinitrogen complexes. Prepared via both reduction and ligand substitution routes, the strength and impact of cation-N_2 interactions have been studied experimentally (IR spectroscopy) and computationally. Although the smallest cation (Li^+) has the largest impact on the ground-state heterobimetallic activation of N_2, solvation interactions are highly competitive and result in low Li^+–(N_2)Mo binding affinities. Thus, although smaller cations can have the largest electronic impact on substrates, these interactions are also the least persistent.

1. Introduction

Secondary coordination sphere interactions have become essential control mechanisms in modern molecular catalysis.[1–4] Systems exploiting these effects typically rely on the use of multifunctional ligand frameworks to facilitate bond rearrangements around catalyst active sites. The ability to use these interactions as control mechanisms is largely due to the evolution in understanding of the importance of often overlooked effects, such as discrete solvation interactions, hydrogen bonding interactions, and charge build-up during bond transformations. In particular, tethering nucleophiles and electrophiles to transition metal complexes to facilitate substrate transformations has led to significant and sometimes unexpectedly large reactivity enhancements.[1,4–11] Most notably, the ability to control proton movement during catalysis has led to the development of new systems for ionic hydrogenation, electrocatalytic hydrogen storage/utilization, and CO_2 reduction.[12–15] Extension of secondary coordination sphere control to simple cations (those that interact primarily electrostatically, such as alkali metals), known to have a profound role in many types of bond transformations, remain underutilized.

The transition elements are among the most versatile metals in their bonding modalities, able to accommodate bonds with a variety of ionicity and covalency. Cations of the s- and p-block elements, on the other hand, have significantly higher ionic bond character, and electrostatic interactions tend to dominate their interactions with ligands. The build-up of anionic charge can be profoundly important in catalytic processes, particularly reactions that involve redox events. Elaborate studies by Yang,[16] DuBois[6,17,18] and Agapie[19,20] have emphasized the profound effects that simple cations can have on substrate transformations. These cations, either alone or in tandem with nucleophiles, have also found extensive use in organic synthesis.[21–24] The Nazarov cyclization, for example, relies on cationic promoters to facilitate electrocyclic rearrangement,[25] and was originally observed with stoichiometric amounts of strong Lewis acids (e.g. $AlCl_3$ or $FeCl_3$). Catalytic protocols for Nazarov-type cyclizations have since been developed that rely on Li^+,[26] Sc^{3+},[27] Ag^+,[28,29] Cu^{2+},[30] and In^{3+}.[31] The use of softer cations appears to be essential for extending reactivity to more elaborate substrates, which may exhibit undesired side-reactions with harsher Lewis acids. Moreover, the salts of smaller weakly-coordinating anions (e.g. OTf^-, BF_4^-) can be strongly affected by poor solvation and ion pairing, both of change the effective electrophilicity of the cationic activator. The strength and nature of the interactions between simple cation electrophiles and potential substrates extends far beyond the cation itself; salt solubility, solvation, and ion pairing all play profound roles in modulating cation electrophilicity (Figure 1).[32]

Figure 1. Equilibria operative during the electrophilic activation of substrates; successful activation requires high solubility of the salt, weak ion pairing, and persistent interactions between cation and substrate.

[a] Department of Chemistry, University of Wyoming, Dept. 3838, 1000 E. University Avenue, Laramie, Wyoming 82071, United States
† Corresponding Author: Dr. Elliott B. Hulley, ehulley@uwyo.edu
Electronic Supplementary Information (ESI) available: Synthetic procedures, Computational details, and crystallographic files. See DOI: 10.1039/x0xx00000x

Weakly-coordinating anions are critical for the catalytic activity of many alkali metal systems, such as perchlorate and fluorinated borate salts,[33] and the use of $LiClO_4$ has been shown to dramatically improve reactivity of electrophile-catalysed reactions that previously required stoichiometric amount of highly potent Lewis acids (e.g. Et_2AlCl).[34-35] Solvation control (via the use of weakly-coordinating *solvents*) can facilitate the generation of effectively "naked" cations,[36] and exploiting cation/anion size mismatches allows electrophile/nucleophile catalysis with unlikely salts (e.g. CsF).[37]

In contrast to what has been developed synthetically, biological systems extensively utilize macroscopic structures to control cation movement and placement during enzymatic processes, particularly Na^+ and K^+.[38–42] Many different enzymatic, cellular, and neurological processes are heavily regulated by simple cations, and size effects can have profound impact on biological activity. Dialkylglycine decarboxylase (DGD), for example, whose function requires alkali metal ion binding near the active site, is activated by the relatively large Rb^+ and K^+ ions but inhibited by smaller cations (Li^+ and Na^+).[39,42] Since the connection between form and function that permeates molecular biology has revealed a great deal of insight in "bioinspired" catalysis,[43–45] it seems only natural to extend such inspiration towards cation control.

Many studies of reactions catalysed by electrophilic simple cations have focused on substrates that are *already* polar, but similar effects on non- or weakly-polarized bonds represent an underexplored field. These effects likely play a substantial role in processes that facilitate activation of one of the weakest-binding substrates, molecular N_2. Fixation of nitrogen is one of the most important chemical reactions for modern life, occurring both on a massive biochemical scale (in the form of the enzyme nitrogenase)[46–53] and a massive industrial scale (as the Haber-Bosch process).[54] Critically, modern industrial operations for heterogeneously-catalysed nitrogen fixation *rely* on the addition of simple cations as catalysis promotors. In fact, modern systems are the result of the fusion of Fe_3O_4-based catalyst beds and different amounts of K_2O, SiO_2, CaO, MgO, and Al_2O_3 promoters.[55,56] Of these materials, potassium serves an "electronic promoter" role, which is localized on the surface of Fe_3O_4. Understanding the exact role of these ionic promoters is crucial for developing new catalysts with better activity, higher selectivity and robostness.[55] A systematic study of the nature of alkali metal/N_2 interactions, with special focus on the ion size and its orientation with respect to a bound dinitrogen ligand, could shed important light on the factors that are most important for alkali metal promotion. The importance of such work has been particularly highlighted by the work of Holland on the multimetallic reduction of nitrogen mediated by molecular iron complexes.[57]

Molecular examples of dinitrogen binding have been the subject of intense study since the original discovery by Allen and Senoff.[58] In the aftermath of this discovery, a great deal of coordination modes and degrees of N-N bond activation have been reported. The nature and extent of N-N bond weakening can be determined structurally (i.e. X-ray crystallography) or spectroscopically (i.e. vibrational spectroscopy) by measuring the N-N vibrational frequency. For weak to moderate activation, N-N vibrational frequencies are typically between 2300 cm^{-1} and 1800 cm^{-1}, and is significantly affected by metal oxidation state and ligand geometry (Figure 2).[53,59–68] Much of the work over the past fifty years has focused on just the effects of the primary coordination sphere, and investigations into the importance of secondary coordination sphere effects and cation interactions have recently gained momentum.

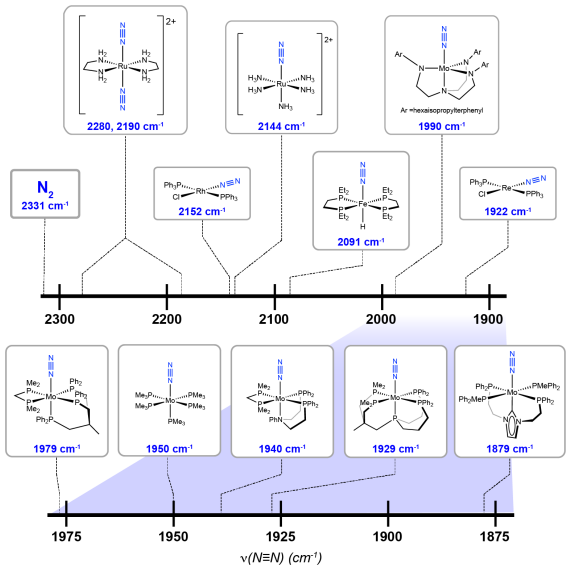

Figure 2. A comparison of transition metal complexes of dinitrogen and their ν(N-N) stretching frequencies (IR or Raman); within a particular family, N_2 stretching frequencies can be modulated by at least 100 cm^{-1}.[57–60,66–68]

A wide variety of interactions between simple cations and metal-bound N_2 ligands have been reported,[57,72–85] most of which have been characterized in the solid state by X-ray crystallography. Efforts to *systematically* study the effects of bifunctional N_2 activation have become of greater importance, although much of the attention has focused on much stronger electrophiles that impart a relatively high degree of covalency (e.g. BR_3, AlR_3, SiR_3^+).[53,86] Many past studies have focused solely on metal and ligand control for N_2 activation, whereas recent studies examine how electrophilic additives further stabilize donation from the transition metal into N_2 (Figure 3). Alkali metal interactions typically lack significant covalency and are thus more labile,[87–89] a property that is actually an asset in catalytic applications due to the Sabatier Principle since catalytic rates are facilitated by both stabilization of high-energy intermediates and *destabilization* of low-energy intermediates – very strong E^+–N_2 interactions would deleteriously bias catalytic applications.[90]

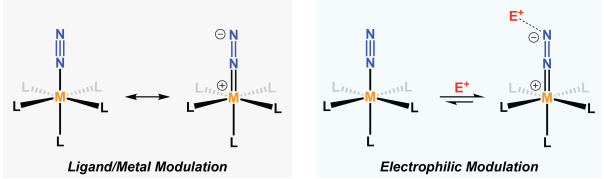

Figure 3. Synthesized ligand platform and application towards heterobimetallic substrates

This report examines the nature of the interactions between tethered alkali metal cations with the dinitrogen ligands of Mo^0 polyphosphine complexes. These systems typically exhibit moderate activation when N_2 is bound to a single Mo center but are sufficiently reducing that anionic charge can be stabilized at the terminal nitrogen via interaction with targeted alkali metals. Based on the precedent established by McLain,[91,92] a family of multidentate lariat-ether phosphine ligands have been developed in order to further investigate the secondary coordination effects of tethered cations on non-polar substrates (Figure 4).[93]

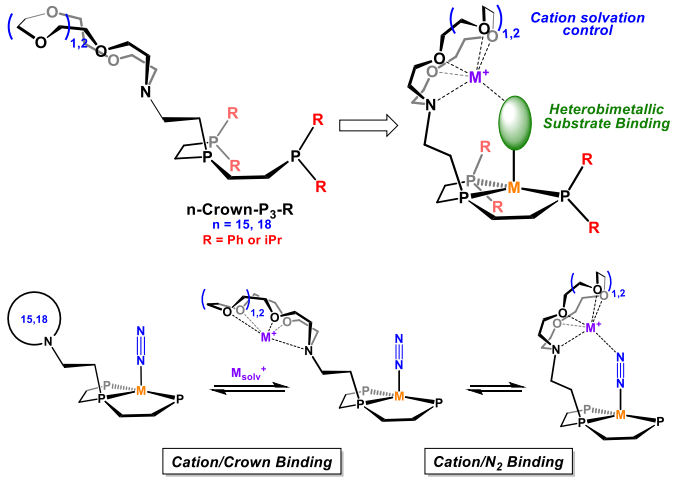

Figure 4. Synthesized ligand platform and application towards heterobimetallic substrates (top) and the binding equilibria relevant to evaluating simple electrophile activation of N_2.

Solvent interactions with salt precursors (i.e. sources of simple cations) must be balanced; strong solvents that lead to high salt solubilities also act as strong ligands that inhibit crown/cation interactions, but weak solvents won't lead to any dissolution. Moreover, due to the variable "solvating" ability of the crown ether, in addition to its conformational flexibility and that of the lariat linker, interactions between dinitrogen the crown-bound cation are modulated by a reversible binding equilibrium. These issues, combined with the need to minimize ion-pairing, required the use of fluorarene solvents and salts of the tetrakis(pentafluoroaryl)borate anions.[94–97]

2. Results and Discussion

2.1 Synthesis of (n-Crown-P_3-R)$MoCl_3$

Several different approaches were employed for the synthesis of zero-valent Mo(N_2) compounds that bear pendant crown ethers. Studies began with traditional reduction routes from Mo(III) precursors;[93] addition of the triphosphine ligands n-Crown-P_3-R (n = 15, 18; R = Ph, iPr) to $MoCl_3(THF)_3$ yields *mer*-(n-Crown-P_3-R)$MoCl_3$ complexes as pale brown/yellow powders in 68-78% crude yields (n= 15, 18; Figure 5, top). The meridional coordination geometry of the tridentate ligand in all four complexes was inferred on the basis of derivatives prepared via addition of salts, HCl, and partial reduction as discussed below.

Heterobimetallic ligand designs often rely on differential binding capacity, and the present case is no exception. A major reason for tethering crown ethers to phosphine frameworks in particular was to ensure regioselectivity of binding of both simple cations and catalytically-relevant transition metal platforms. This framework presents two major challenges for synthesis; firstly, conformational flexibility leads to a profound resistance to crystallization, and secondly metalation of n-Crown-P_3-R ligands with more oxophilic elements (such as Mo) is complicated by a lack of binding specificity. Despite varying the synthetic conditions (temperature, order of addition, excess ligand), it seems that products invariably contained small amounts of product with Mo^{III} bound to the crown ether. This is supported by the observations that the powdered products isolated from ligand exchange reactions repeatedly exhibited systematically lower C/H/N elemental compositions than calculated and that magnetic measurements using the Evans method routinely yielded higher magnetic moments than expected for a single Mo^{III}. Addition of an equivalent of $MoCl_3(THF)_3$ to ~95% pure *mer*-(15-Crown-P_3-Ph)$MoCl_3$ resulted in the formation of a new compound, evidenced profound shifts in the crown-ether protons (Figure S1).

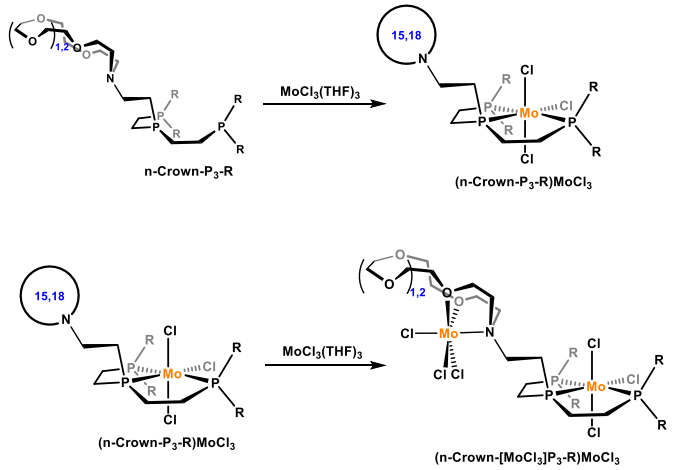

Figure 5. Synthesis of *mer*-(n-crown-P_3-R)$MoCl_3$ readily occurs *via* ligand substitution of $MoCl_3(THF)_3$ (top), but formation of pure products is complicated by additional Mo coordination at the crown ether (bottom).

Despite significant effort, crystalline products have been rare and usually occur as the result of decomposition or side reactivity. For example, the trichloride complexes (n-Crown-P_3-iPr)$MoCl_3$ (n = 15, 18) themselves manifest as brown/yellow powders that resist crystallization, but washing samples of both derivatives with Et_2O resulted in light ether yellow solutions that yielded small amounts of yellow pyramidal crystals upon evaporation. Crystals resulting from washing both derivatives were amenable to X-ray crystallographic analysis, revealing that the yellow solution contained the complexes as their HCl salts [(n-Crown[H^+]-P_3-iPr)$MoCl_3$]Cl (Figure 6, top). Although the structure of [(15-Crown[H^+]-P_3-iPr)$MoCl_3$]Cl could not be completely solved due to crown ether disorder, the overall framework and exogenous chloride were visible in difference

maps (Figure 6). The origin of the HCl is not known at present, but the most obvious sources are either (1) contaminated starting material or (2) decomposition.

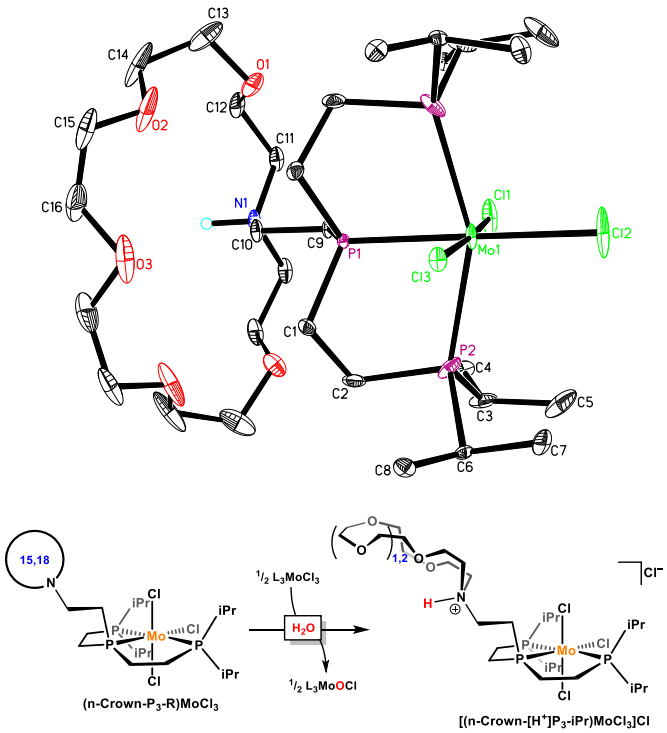

Figure 6. Proposed degradation of (n-Crown-P_3-iPr)$MoCl_3$ *via* reaction with trace amounts of H_2O resulting in formation of the hydrochloride salt [(n-Crown[H^+]-P_3-iPr)$MoCl_3$]Cl (top, m = 1, 2) as revealed by the solid state structure of [(18-Crown[H^+]-P_3-iPr)$MoCl_3$]Cl (bottom). Hydrogen atoms and an exogenous chloride anion have been omitted for clarity.

Although it is conceivable that the $MoCl_3(THF)_3$ starting material is contaminated with HCl or CH_2ClCN, which are by-products of the formation of its precursor $MoCl_4(NCCH_3)_2$ from $MoCl_5$, the subsequent reduction with Sn^0 and purification steps would likely eliminate both.[98] The more likely source of HCl is adventitious water, which would rapidly hydrolyze the L_nMoCl_3 species to produce $[L_nMoOCl]_m$ oxychlorides and HCl (Figure 6, bottom).[99]

2.2 Synthesis of (n-Crown-P_3-R)$Mo(N_2)L_m$ Complexes by Reduction and Ligand Substitution

Numerous different reduction strategies (Na/Hg, Mg) were applied to perform a successful reduction of these Mo^{3+} precursors to obtain Mo^0 dinitrogen complexes, although these routes met with mixed success. For example, attempts to reduce *mer*-(18-Crown-P_3-R)$MoCl_3$ with excess Na/Hg or Mg^0 in the presence of PPh_2Me resulted in a mixture of products including $Mo(N_2)_2(PPh_2Me)_4$. The failure of this synthesis did not result Mo-Mo bond formation, as partial reduction to the Mo^{II} complex *mer*-(18-Crown-P_3-R)$MoCl_2(PPh_2Me)$ (Figure 7). Although *direct* structural proof remains elusive, complexation addition of $Ca(OTf)_2$ to the reduced product and slow evaporation led to the formation of orange/yellow crystals of the adduct *mer*-(18-Crown[$Ca(OTf)_2$]-P_3-Ph)$MoCl_2(PPh_2Me)$.

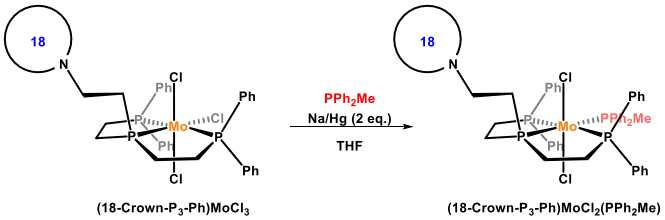

Figure 7. Synthesis of (18-Crown-P_3-Ph)$MoCl_2(PPh_2Me)$ via Na/Hg reduction.

X-Ray crystallographic characterization confirmed the binding of $Ca(OTf)_2$ to the crown ether and that the meridional geometry the triphosphine ligand was conserved (Figure 8). Chelating phosphines presented mixed results. Reducing trichloride precursors in the presence of bis(diphenylphosphino)ethane (dppe) ligand produced a large mixture of products with no clear majority component.

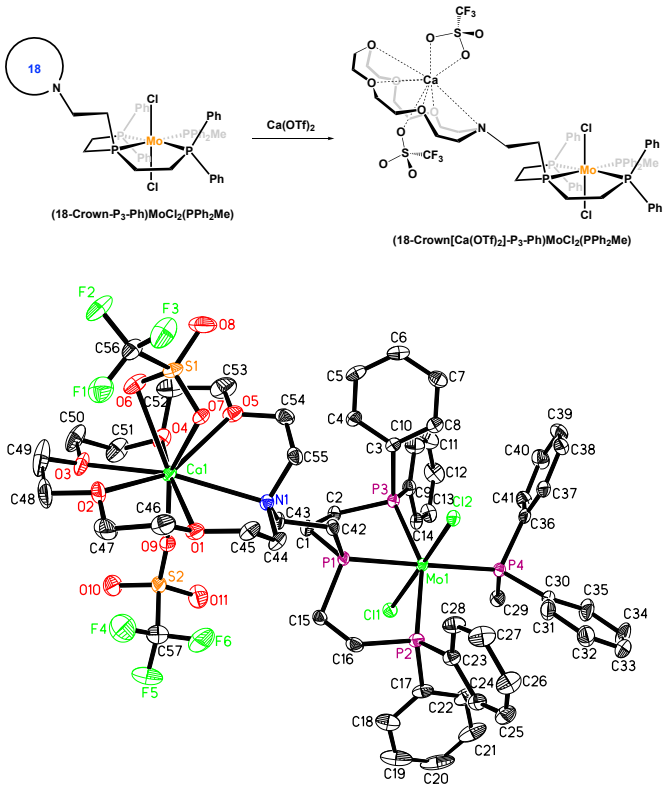

Figure 8. Synthesis of of (18-Crown[$Ca(OTf)_2$]-P_3-Ph)$MoCl_2(PPh_2Me)$ Crystal structure of (18-Crown[$Ca(OTf)_2$]-P_3-Ph)$MoCl_2(PPh_2Me)$. Hydrogen atoms, toluene solvates, and the second set of sites for the disordered O3, C50, C51, and O4 have been omitted for clarity.

Bite angle appears to play a substantial role; reduction of *mer*-(18-Crown-P_3-Ph)$MoCl_3$ with excess Na/Hg amalgam (10 eq.) in the presence of bis(diphenylphosphino)methane led to the clean production of *fac*-(18-Crown-P_3-Ph)$Mo(N_2)$(dppm). Stereochemical assignment is made based on the lack of significant *trans* ^{31}P-^{31}P coupling to the central phosphine (which manifests as a triplet of triplets, J_{PP} = 13 Hz and 4 Hz) and the similarity in the remaining coupling pattern with (triphos)$Mo(N_2)$(dppm) (Figure 9).[71] As with *trans*-$Mo(N_2)_2(PPh_2Me)_4$, the arylphosphine ligands in *fac*-(18-Crown-P_3-Ph)$Mo(N_2)$(dppm) are disposed in a mutually equatorial fashion, placing the lariat-bearing phosphine *trans* to the

dinitrogen ligand and rendering the crown incapable of supporting alkali metal/N_2 interactions.

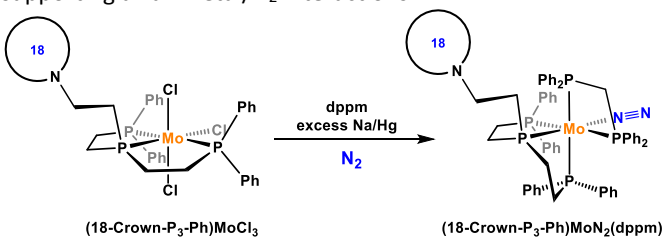

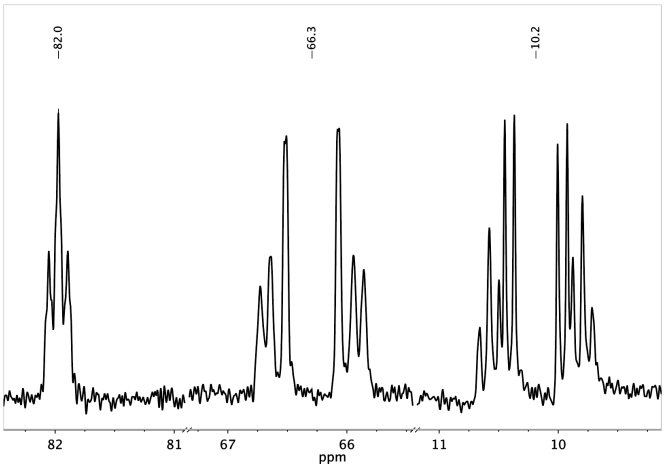

Figure 9. Synthesis of *fac*-(18-Crown-P_3-Ph)Mo(N_2)(dppm) from *mer*-(18-Crown-P_3-Ph)$MoCl_3$ and its $^{31}P\{^1H\}$ NMR spectrum highlighting the pseudo-C_s symmetry of the complex.

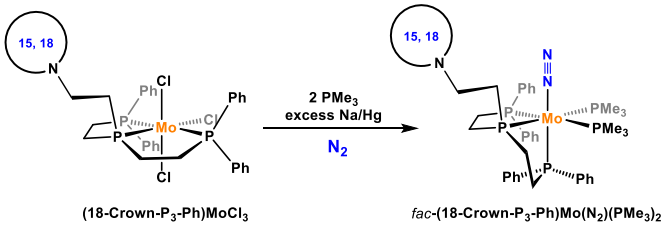

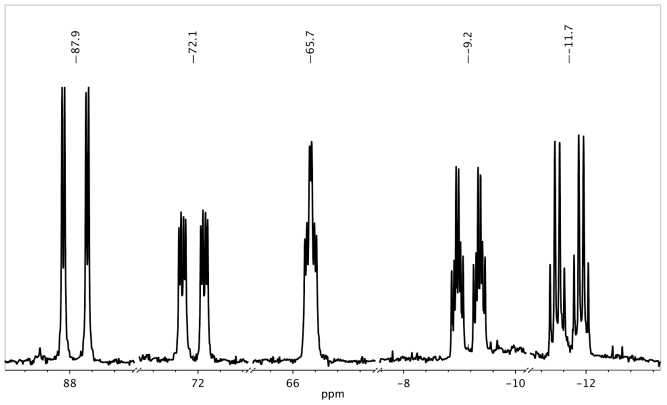

Figure 10. Synthesis of *fac*-(n-Crown-P_3-Ph)Mo(N_2)(PMe_3)$_2$ from *mer*-(n-Crown-P_3-Ph)$MoCl_3$ (n = 15, 18; top) and the $^{31}P\{^1H\}$ NMR spectrum of *fac*-(18-Crown-P_3-Ph)Mo(N_2)(PMe_3)$_2$ highlighting the C_1 symmetry of the complex.

Reduction of trichloride precursors in the presence of PMe_3 produced the most satisfactory results. Exposure of *mer*-(n-Crown-P_3-Ph)$MoCl_3$ (n = 15, 18) to excess Na/Hg (>10 eq) in the presence of PMe_3 (2 eq) resulted in a crude mixture that contained *fac*-(n-Crown-P_3-Ph)Mo(N_2)(PMe_3)$_2$, *cis*- and *trans*-Mo(N_2)$_2$(PMe_3)$_4$, and Mo(N_2)(PMe_3)$_5$. The side products were separated *via* extraction with MeOH/hexane, resulting in clean isolation of *fac*-(n-Crown-P_3-Ph)Mo(N_2)(PMe_3)$_2$ as yellow/brown oils (Figure 10). Stereochemical assignment is made on the basis of the symmetry and coupling patterns observable in the $^{31}P\{^1H\}$ NMR spectra of both complexes.

Despite having the ^{i}Pr-substituted derivatives n-Crown-P_3-iPr in hand (n = 15, 18),[93] reduction approaches using these more sterically-encumbered frameworks failed to produce clean products and ligand substitution reactions were instead employed.[100] Over the course of 24h in THF solution, Mo(N_2)$_2$(PPh_2Me)$_4$ and (n-Crown-P_3-R) react cleanly at room temperature to produce *mer*-(n-Crown-P_3-R)Mo(N_2)$_2$(PPh_2Me) (Figure 11; n = 15, 18; R = Ph, iPr). Isolation of the products from free PPh_2Me was accomplished by silica chromatography; the product mixture was layered onto a pad of silica in the glovebox and PPh_2Me was eluted with copious amount of toluene, followed by elution with THF and concentration of the THF-soluble phase. The sticky, dark-brown *mer*-(n-Crown-P_3-R)Mo(N_2)$_2$(PPh_2Me) products were clean by $^{31}P\{^1H\}$ NMR spectroscopy and used without any further purification.

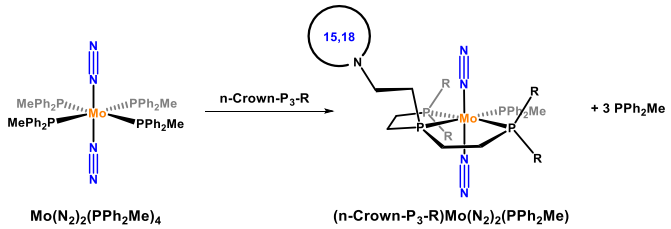

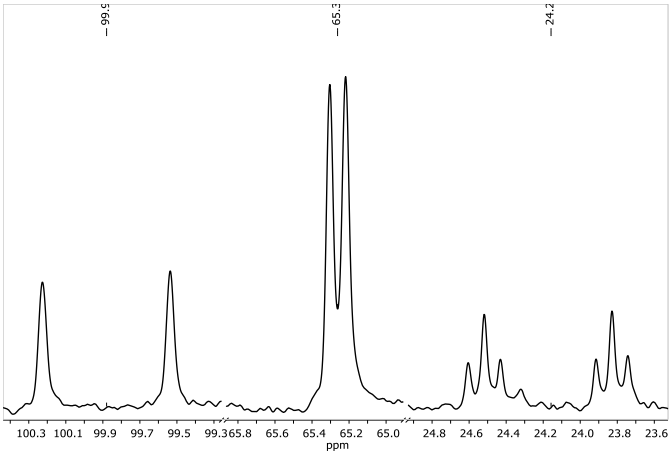

Figure 11. Synthesis of (n-Crown-P_3-^{i}Pr)Mo(N_2)$_2$(PPh_2Me) via ligand substitution and its $^{31}P\{^1H\}$ NMR spectrum.

2.3. Interactions Between Mo-bound N_2 and Tethered Alkali Metals: FTIR Spectroscopic Investigations

Crown ethers have well-known binding selectivities,[93,101–103] where the ring size strongly correlates with relative cation binding affinities, but this relative selectivity is often overshadowed by the very strong affinities that crown ethers have for cations of any size.[91,101] As utilized here, these rings are

better thought of as microsolvation environments wherein the ring size and number of donor atoms tunes the availability of cations for electrophile reactivity. Of the solvents tested, weakly-binding (but polar) fluoroaryl solvents were the most effective, and the bulk of the work presented here were performed in *ortho*-difluorobenzene (ODF) using salts of the tetrakis(pentafluorophenyl) borate anion as cation sources ($M^+[BF_{20}^-]$, $M^+ = [Li(OEt_2)_4]^+$, Na^+, K^+, Rb^+, Cs^+).[97]

2.3.1 Alkali metal coordination in *fac*-(n-Crown-P_3-Ph)Mo(N_2)(PMe_3)$_2$ complexes

Solution-phase IR spectra of these compounds develop complexity upon addition of alkali metal cation sources (e.g. $M^+[BF_{20}^-]$) that, taken together, are particularly revealing of direct alkali metal/N_2 interactions. Addition of alkali metal salts to crown-bearing Mo(N_2) complexes is complicated by two possible equilibria (Figure 12); the first involves exchange between solvated cations and the crown ether (K_{desolv}) and the second involves the interaction of interest (K_{bind}). NMR spectroscopy has revealed that K_{desolv} is likely larger than unity, as the ^{1}H NMR resonances associated with the crown ethers change dramatically upon mixing with alkali metal salts. IR spectroscopy of the salted complexes are consistent with the observation of both the bound and unbound isomers, with relative concentrations that depend on the alkali metal cation. Addition of BF_{20} salts to *fac*-(15-Crown-P_3-Ph)Mo(N_2)(PMe_3)$_2$ yields a major $\nu(N_2)$ stretching frequency at 1950 cm^{-1} (at essentially the same position as the unsalted derivative) but as the series progresses from Li^+ to Cs^+, what starts as a broad shoulder centred around 1915 cm^{-1} (for Li^+) becomes a dominating feature around 1934 cm^{-1} (for Cs^+).

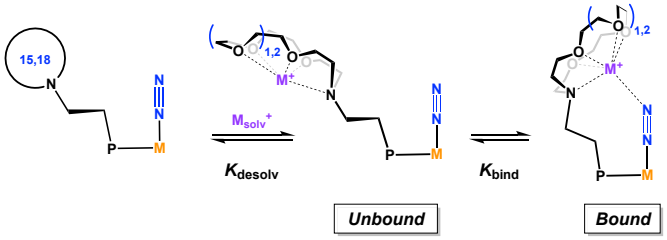

Figure 12. Two equilibria are relevant to the present study, K_{desolv} and K_{bind}, although NMR and IR spectroscopy reveal that K_{desolv} is likely large K_{bind} is likely the limiting factor in terms of facilitating alkali metal interactions with bound N_2.

Fitting simple gaussian curves to the IR spectra results in tentative assignments of the stretching frequencies for the unbound and bound isomers of the salted complexes. Naturally there is a rather large uncertainty in the stretching frequencies of gaussian components (~ 15 cm^{-1}), but the values extracted from the fits are consistent with frequency shifts ($\Delta\nu(N_2)$ = $\nu(N_2)_{unbound}$ - $\nu(N_2)_{unbound}$) calculated by DFT (see below). A similar trend is observed for the larger crown derivative *fac*-(18-Crown-P_3-Ph)Mo(N_2)(PMe_3)$_2$, although the relative intensities of the bound and unbound isomers are slightly different. For the 15-crown derivative, the relative amount of bound isomer appears to grow as cation size increases, maximizing for Rb^+ before decreasing slightly for Cs^+.

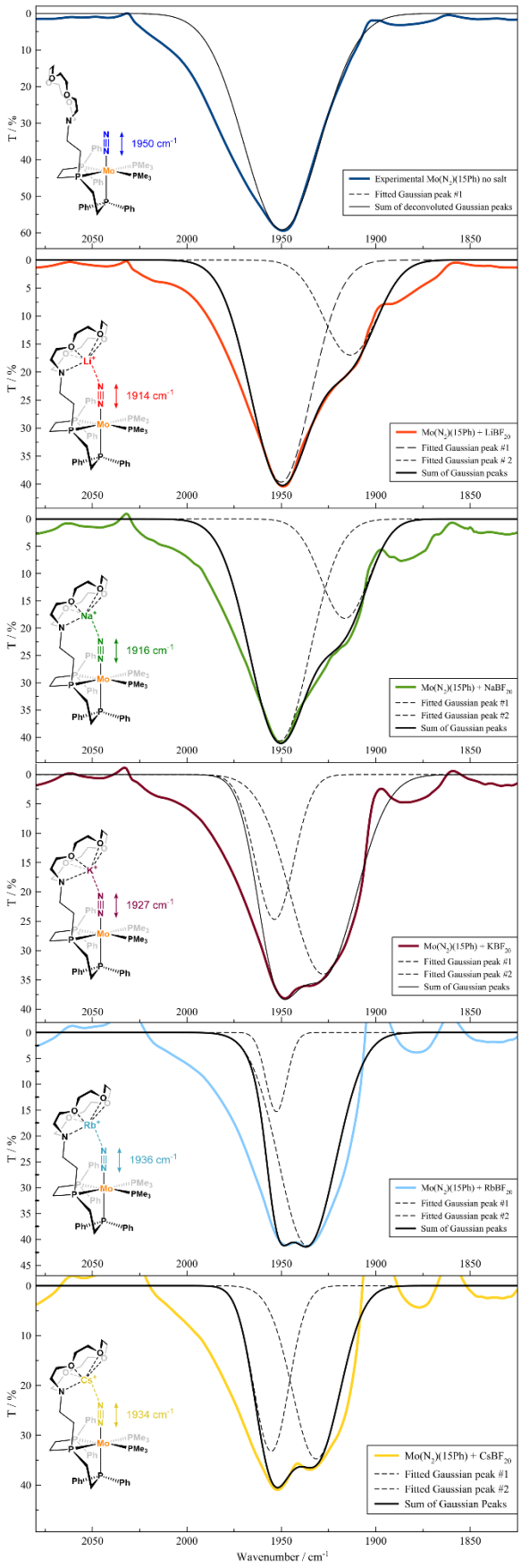

Figure 13. Solution-phase IR spectra of the N_2 vibration region of [(15-Crown-[M^+]-P_3-Ph)Mo(N_2)(PMe_3)$_2$][BF_{20}] salt adducts (M = Li, Na, K, Rb, Cs) in ODF. The peak-like 'features' below 1900 cm^{-1} are due to solvent subtraction artifacts.

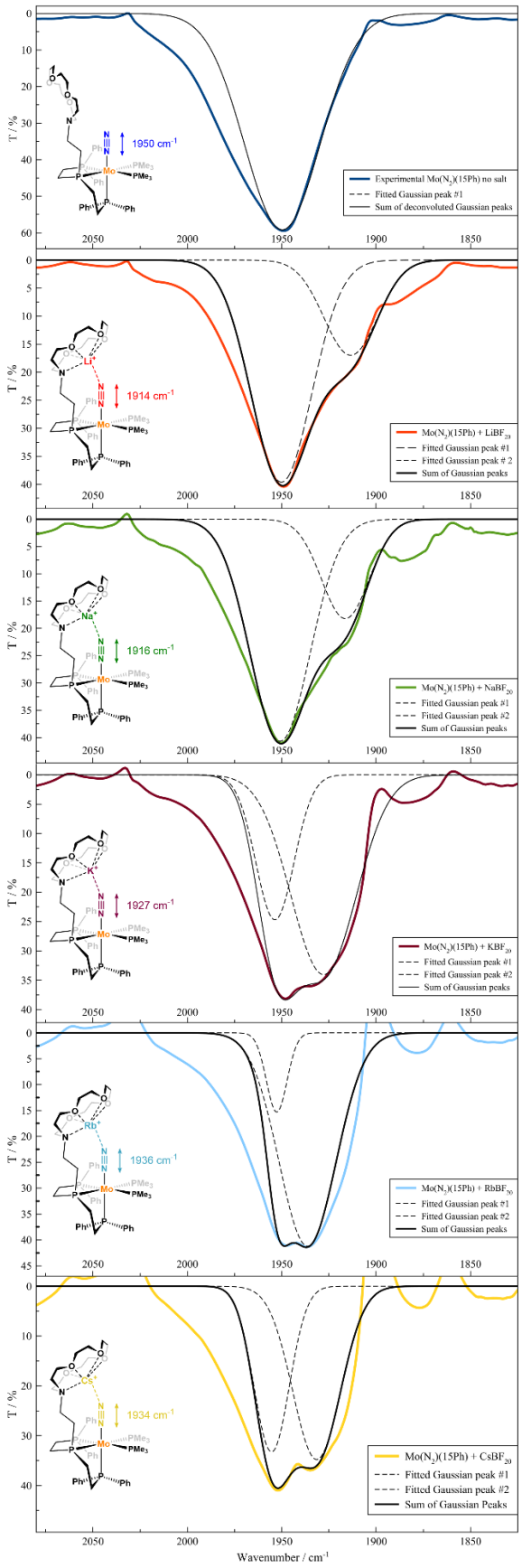

Figure 14. Solution-phase IR spectra of the N_2 vibration region of [(18-Crown-[M^+]-P_3-Ph)Mo(N_2)(PMe_3)$_2$][BF_{20}] salt adducts (M = Li, Na, K, Rb, Cs) in ODF. The peak-like 'features' below 1900 cm^{-1} are due to solvent subtraction artifacts.

Table 1. Tabulated $\upsilon(N_2)$ stretching frequencies for (n-Crown-P_3-Ph)Mo(N_2)(PMe_3)$_2$ (n = 15, 18) as a function of added salt, with the difference between the bound and unbound N_2 stretches indicated ($\Delta\nu(N_2) = \nu(N_2)_{unbound} - \nu(N_2)_{unbound}$)

	fac-(15-Crown-P_3-Ph)Mo(N_2)(PMe_3)$_2$ $\upsilon(N_2)$ (cm^{-1})			*fac*-(18-Crown-P_3-Ph)Mo(N_2)(PMe_3)$_2$ $\upsilon(N_2)$ (cm^{-1})		
	unbound	**bound**	**$\Delta\upsilon(N_2)$**	**unbound**	**bound**	**$\Delta\upsilon(N_2)$**
no salt	1950	-		1952	-	-
$LiBF_{20}$	1951	1914	**37**	1957	1935	**22**
$NaBF_{20}$	1950	1916	**34**	1952	1925	**27**
KBF_{20}	1954	1927	**27**	1951	1931	**20**
$RbBF_{20}$	1953	1936	**17**	1957	1936	**21**
$CsBF_{20}$	1954	1934	**20**	1954	1934	**20**

Clearly the significance of cation-dinitrogen interactions *increases* as the cation size increases, suggesting that the favorability of binding (ΔG_{bind}) has the same size dependence. As the smallest and most electrophilic cation, Li^+ might be assumed to have the strongest interaction with a Mo-bound N_2 ligand (stabilizing the most anionic charge at the terminal nitrogen), but the Li^+ is also likely to be the most stabilized by the crown ether. The size "mismatch" with Li^+ also leads to the possibility of multiple energetically-equivalent isomers and the effective broadening of the vibration of the Li^+-N≡N-Mo interaction, though DFT studies support the possibility that ΔG_{bind} is positive. In contrast, rubidium and cesium are so large (with ionic radii of 1.66 Å and 1.81 Å, respectively)[104] that there is a substantial 'puckering' out of the plane of the rings of 15- and 18-member crown ethers.[101] As a result, these larger ions are considerably more exposed and can more strongly interact with the dinitrogen ligand.

2.3.2 Alkali Metal Coordination in *mer*-(n-Crown-P_3-iPr)Mo(N_2)$_2$(PPh_2Me) Complexes

The bis(dinitrogen) complexes (n-Crown-P_3-iPr)Mo(N_2)$_2$(PPh_2Me) (n = 15, 18) present unique challenges and opportunities to investigate M^+-N≡N-Mo interactions via vibrational spectroscopy. Dinitrogen ligand vibrational stretches couple to each other to yield symmetric and asymmetric absorptions, whose intensity strongly depends on the symmetry of the complex. Although the symmetric coupling mode of the two N_2 ligands ($\nu(N_2)_{sym}$) is ordinarily not visible in IR, the lariat arm of the middle phosphine in n-Crown-P_3-iPr breaks the symmetry and renders $\nu(N_2)_{sym}$ weakly visible. For both the 15- and 18-crown systems, there is little observable effect in the IR spectra upon addition of Li^+, Na^+, or K^+ salts, although weak shoulders begin to manifest for K^+. Addition of Rb^+ and Cs^+ result in more obvious changes, and two new peaks (consistent with a new bis(dinitrogen) complex) begin to appear. The smaller 15-crown ligand exhibits this change more significantly than the larger 18-crown ligand, although the trend is observable in both. A tabulation of the data extracted from gaussian fits to the IR spectra are presented in Tables 2 and 3. There is considerable fitting error due to the broad absorptions

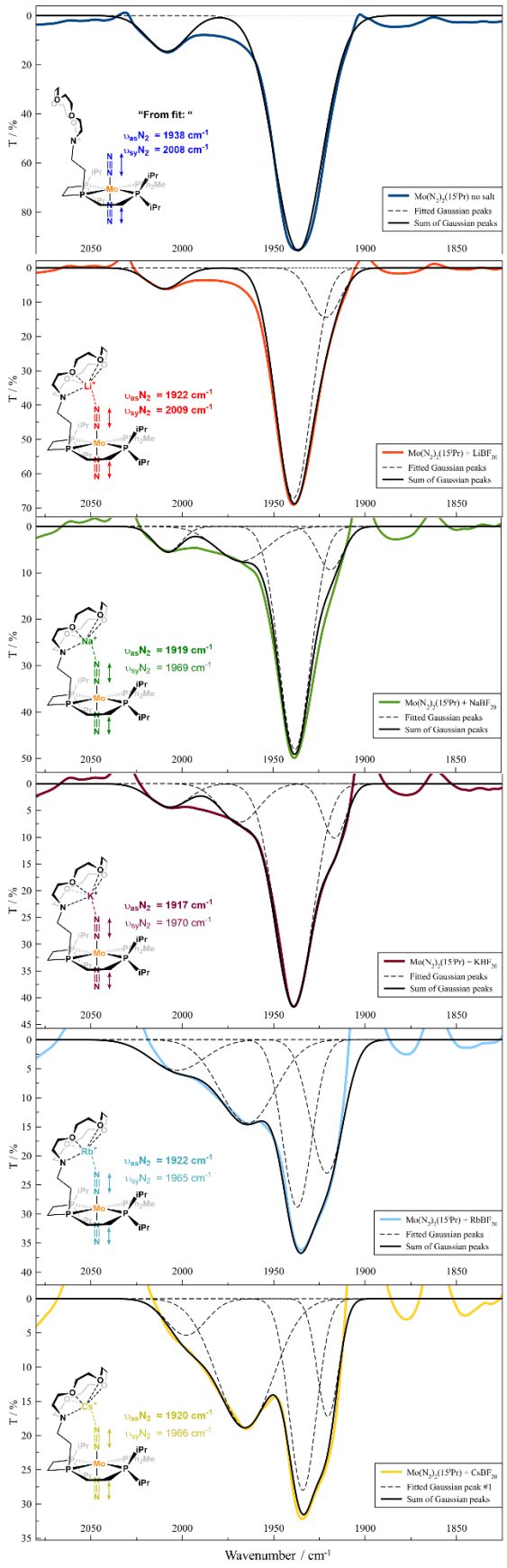

Figure 15. υN_2 asymmetric and symmetric vibrations of different (15-Crown-[MBF_{20}]-P_3-iPr)Mo(N_2)$_2$(PPh_2Me) adducts

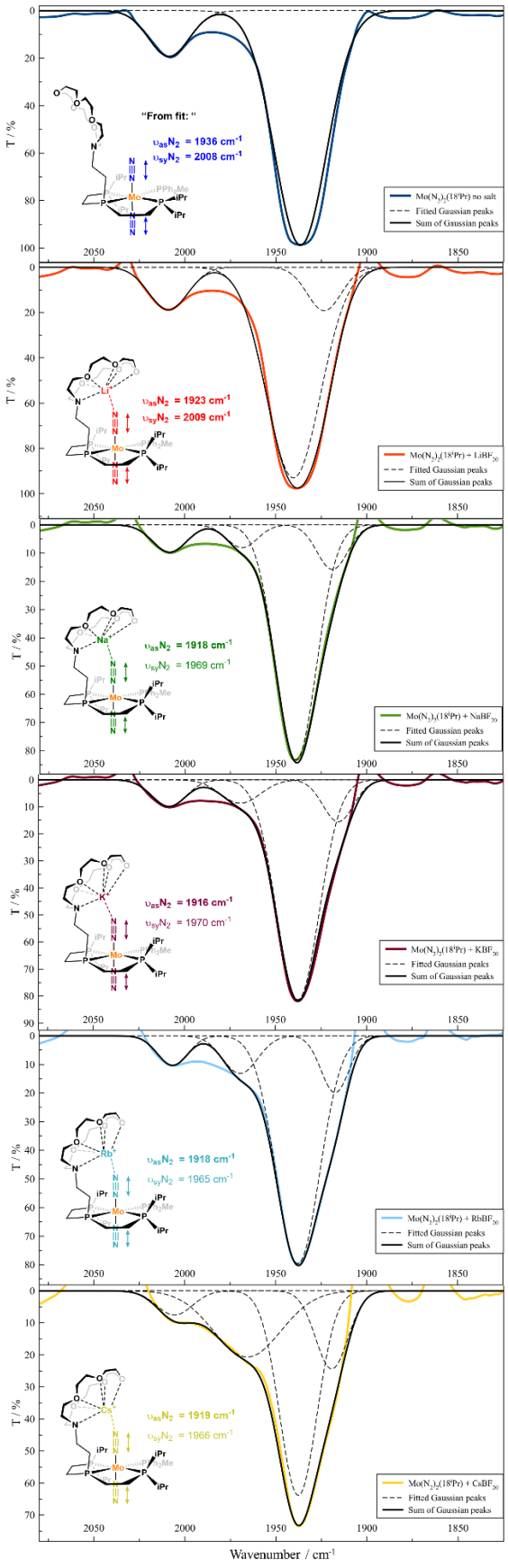

Figure 16. υN_2 asymmetric and symmetric vibrations of different (18-Crown-[MBF_{20}]-P_3-iPr)Mo(N_2)$_2$(PPh_2Me) adducts

Table 2. Experimental stretching frequencies for the antisymmetric N-N stretch of the unbound and bound *mer*-(n-Crown-P_3-Ph)Mo$(N_2)_2$(PPh_2Me) (n = 15, 18) as extracted from IR spectra.

	mer-(15-Crown-P_3-iPr)Mo$(N_2)_2$(PPh_2Me) $\upsilon_{as}(N_2)$ (cm^{-1})			(*mer*-(18-Crown-P_3- iPr)Mo$(N_2)_2$(PPh_2Me) $\upsilon_{as}(N_2)$ (cm^{-1})		
	unbound	**bound**	**$\Delta\upsilon N_2$**	**unbound**	**bound**	**$\Delta\upsilon N_2$**
no salt	1938	-	-	1936	-	-
$LiBF_{20}$	1938	-	-	1940	-	-
$NaBF_{20}$	1939	1919	**20**	1939	1918	**21**
KBF_{20}	1939	1917	**22**	1938	1916	**22**
$RbBF_{20}$	1938	1922	**16**	1938	1918	**20**
$CsBF_{20}$	1934	1920	**14**	1938	1919	**19**

Table 3. Experimental stretching frequencies for the symmetric N-N stretch of the unbound and bound *mer*-(n-Crown-P_3-Ph)Mo$(N_2)_2$(PPh_2Me) (n = 15, 18) as extracted from IR spectra.

	mer-(15-Crown-P_3-iPr)Mo$(N_2)_2$(PPh_2Me) $\upsilon_{sy}(N_2)$ (cm^{-1})			(*mer*-(18-Crown-P_3- iPr)Mo$(N_2)_2$(PPh_2Me) $\upsilon_{sy}(N_2)$ (cm^{-1})		
	unbound	**bound**	**$\Delta\upsilon N_2$**	**unbound**	**bound**	**$\Delta\upsilon N_2$**
no salt	2008	-	-	2008	-	-
$LiBF_{20}$	2009	-	-	2009	-	-
$NaBF_{20}$	2008	1967	**41**	2008	1968	**40**
KBF_{20}	2007	1970	**37**	2009	1969	**40**
$RbBF_{20}$	2004	1965	**39**	2007	1969	**38**
$CsBF_{20}$	1998	1966	**32**	2006	1966	**40**

and peak overlap, so these values have been taken as estimates. The general trend for the bis(dinitrogen) complexes is similar to that for the mono(dinitrogen) complexes – as the cation size increases, the favourability of binding the crown-tethered cation to the Mo-bound N_2 ligand increases. Both the symmetric and antisymmetric N_2 stretching frequencies red-shift upon coordination, but the symmetric shift is significantly more affected.

2.3.3 DFT Studies of Alkali Metal Coordination

To lend support to $\nu(N_2)$ stretching frequency assignments and binding equilibria, DFT studies were performed on the mono- and bis-dinitrogen complexes discussed above. The hybrid meta-exchange correlation functional M06-L (in concert with the def2-TZVP basis set) was employed to get reasonable estimates for the alkali metal binding energies; Effective Core Potentials (ECPs) were used for Mo, Rb and Cs atoms.[105,106] The large degrees of freedom required a degree of structural simplification to achieve convergence in reasonable time frames. For the mono-dinitrogen complexes bearing facially-coordinating ligands, the phenyl substituents on the terminal phosphine arms presented problems in terms of computational cost and a resistance to optimization convergence, so these groups were truncated to methyl groups. The stereochemical requirements for facial coordination are such that truncation of the phenyl substituents should yield minimal steric differences, although the increase in donor strength for the phosphine arms may result in a slight underestimate of the strength of M^+–N_2 binding (i.e. the calculated ΔG_{bind} for R = Ph would likely be more negative). It is important to note that using a continuum solvation model means ignoring the importance of explicit solvation of the cations on *both* sides of the unbound/bound equilibrium. Due to that fact, and the usual level of discrepancy between DFT-derived values and experiments, the calculated ΔG_{bind} values are presented here only to reflect the general agreement between the experimental IR data and the calculated values.

The calculated stretching frequency changes upon alkali metal coordination ($\Delta\upsilon(N_2)_{calc}$) agree with the proposed assignments discussed above. For the mono(dinitrogen) complexes, Li^+ incurs the largest shift in the dinitrogen stretching frequencies for both the 15-crown and 18-crown complexes but binding to the dinitrogen itself is predicted to be slightly endergonic (Table 4).

Table 4. Calculated vibrational data and binding energy for the truncated mono(dinitrogen) system (*fac*-(n-Crown-P_3-Me)Mo$(N_2)(PMe_3)_2$ (n = 15, 18))

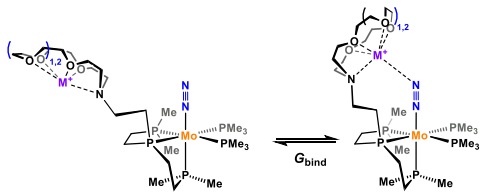

***fac*-(15-Crown-P_3-Me)Mo$(N_2)(PMe_3)_2$**					
	Li^+	**Na^+**	**K^+**	**Rb^+**	**Cs^+**
$\upsilon(N_2)_{bound}$	1941	1958	1964	1979	1981
$\Delta\upsilon(N_2)_{calc}$	-55	-47	-48	-17	-17
ΔG^0_{bind} kcal mol^{-1}	**6.20**	**-2.72**	**-6.63**	**-0.11**	**-3.50**
***fac*-(18-Crown-P_3-Me)Mo$(N_2)(PMe_3)_2$**					
	Li^+	**Na^+**	**K^+**	**Rb^+**	**Cs^+**
$\upsilon(N_2)_{bound}$	1950	1966	1971	1963	1959
$\Delta\upsilon(N_2)_{calc}$	-35	-19	-13	-21	-36
ΔG^0_{bind} kcal mol^{-1}	**3.56**	**1.31**	**1.30**	**-2.17**	**-2.81**

Of all the alkali metals studied, Li^+ also incurred the largest change of the N-N distance upon binding (1.150 Å bound vs. 1.139 Å unbound), but the significant conformational flexibility leads to a relatively flat potential energy surface, and many of the structures calculated only converged after a great deal of time and usually several re-starts. For that reason, the calculated bond distances are not likely to be representative of the structures operative in experiments. Moreover, although the correlation between cation size and binding energy (ΔG_{bind}) is weak, the values themselves are relatively modest (between +6 and –6 kcal/mol) and the lack of a strong trend is probably a reflection of (1) the large number of conformers possible for small ions in large crowns and (2) steric interactions between the crown and the phosphine arms.

Calculations on the meridionally-coordinated bis(dinitrogen) complexes were somewhat less helpful, although generally consistent with the experimental observations (Table 3 and 5). The isopropyl substituents presented less complications when it came to geometry optimizations, so calculations on the full

structures were performed. Although "bound" structures for complexes bearing Li^+, Na^+, and K^+ cations could be found, the minimized structures possessed such long M^+-N_2 bond lengths (longer than the sum of the van der Waals radii) that these are not likely to truly reflect any real bonding interaction. Accordingly, the calculated N_2 stretching frequencies are only weakly perturbed from the 'unbound' structures, particularly in the 15-crown derivative. Even the calculated Rb^+ and Cs^+ structures appear to inhabit a space quite far away from the N_2 ligand, farther than might expected on the basis of their impacts on $\upsilon(N_2)$ stretching frequencies.

Table 5. Calculated vibrational data and cation binding strength for the truncated bis(dinitrogen) system *mer*-(n-Crown-P_3- iPr)$Mo(N_2)_2(PPh_2Me)$ (n = 15, 18), wherein the symmetric ('sym') and antisymmetric ('as') stretches. Asterisks denote metals for which M^+–N interactions are significantly longer than the van der Waals radii due to steric repulsion from the iPr groups.

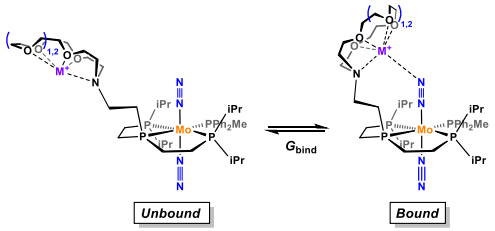

***mer*-(15-Crown-P_3-iPr)$Mo(N_2)_2(PPh_2Me)$**					
	Li^{+*}	Na^{+*}	K^{+*}	Rb^+	Cs^+
$\upsilon(N_2)_{sym/Unbound}$	2070	2072	2070	2072	2075
$\upsilon(N_2)_{sym/Bound}$	2075	2076	2076	2067	2069
$\Delta\upsilon(N_2)_{calc}$	5	5	6	-6	-6
$\upsilon(N_2)_{as/Unbound}$	2005	2005	2005	2006	2010
$\upsilon(N_2)_{as/Bound}$	2010	2011	1998	1995	1997
$\Delta\upsilon(N_2)_{calc}$	4	6	-7	-11	-13
ΔG^0_{bind} kcal mol^{-1}	**2.71**	**4.07**	**1.49**	**1.12**	**1.61**
***mer*-(18-Crown-P_3- iPr)$Mo(N_2)_2(PPh_2Me)$**					
	Li^{+*}	Na^{+*}	K^{+*}	Rb^+	Cs^+
$\upsilon(N_2)_{sym/Unbound}$	2075	2076	2073	2077	2072
$\upsilon(N_2)_{sym/Bound}$	2073	2074	2071	2068	2066
$\Delta\upsilon(N_2)_{calc}$	-2	-2	-2	-9	-6
$\upsilon(N_2)_{as/Unbound}$	2009	2010	2007	2007	2007
$\upsilon(N_2)_{as/Bound}$	1987	1992	1997	1991	1992
$\Delta\upsilon(N_2)_{calc}$	-22	-19	-10	-16	-15
ΔG^0_{bind} kcal mol^{-1}	**2.37**	**–2.34**	**1.57**	**0.18**	**-4.90**

Nonetheless, this is consistent with the experimental observation that Li^+, Na^+, and K^+ have only negligible effects and that Rb^+ and Cs^+ show modest interactions. The fact that the binding interactions (both calculated and experimental) are uniformly weaker for the meridonal complexes can be ascribed to the significant steric constraints of the isopropyl groups on the phosphorus arms. These repulsive interactions are rendered more significant for meridonal coordination, since these groups flank the dinitrogen ligand on both sides.

2.4 Reactivity of $Mo(N_2)$ Complexes with p-Block Cations

In an attempt to study the effects of stronger covalent interactions on N_2 activation, the BF_{20}^- salts of Ag^+ and Tl^+ were prepared and their reactivity with the lariat-ether $Mo(N_2)$ complexes was studied. Exposure of *any* of the previously discussed $Mo(N_2)$ complexes (i.e. *fac*-(n-Crown-P_3-Ph)$Mo(N_2)(PMe_3)_2$ and *mer*-(n-Crown-P_3-iPr)$Mo(N_2)_2(PPh_2Me)$) to a slight excess (1.1 eq.) of either $Ag[B(C_6F_5)_4]$ or $Tl[B(C_6F_5)_4]$ led to nearly immediate oxidation of the Mo complex and precipitation of reduced Ag^0 or Tl^0. Oxidation by Ag^+ is well precedented in synthetic chemistry, but the Tl^+ reactivity was at first surprising since thallous salts are generally used to *avoid* oxidation chemistry. Comparison of the aqueous redox potentials of Ag^+ and Tl^+ (0.79 V and –0.34 V vs. NHE, respectively) with the known THF redox potentials of $Ag^{+/0}$ and phosphine-ligated $Mo^0(N_2)$ complexes (+0.63 V and ≤ –1 V vs. Fc/Fc^+, respectively) suggest that Tl^+ is indeed a strong enough oxidant to degrade the N_2 complexes studied. Electrostatic interactions are clearly insufficient when employing cations that incur a significant amount of covalency; such systems would likely require softer ligand frameworks (e.g. incorporating S-atoms to make thiacrown derivatives).

2.5 The Interplay of Crown Size, Cation Size, and Crown Positioning

The crown ethers employed in this study act as models of a microsolvation environment. For much smaller cations (like Li^+), the 15- and 18-crown macrocycles are relatively large and provide enough O- and N-atom donors to compete effectively with the weak interactions. Although crystallographic evidence in the present study is insufficient, dozens of other studies have shown that as cations get larger, they fail to fit completely within the constraints of the ring.[107–116] For example, in known systems of 15-crown-5 the large cations Rb^+ and Cs^+ are relatively exposed and can protrude >2Å beyond the plane of the ring whereas smaller Li^+ and Na^+ are nearly coplanar (depending on coligands). When puckered out of the ring, the effectiveness of the donor atoms decreases and the alkali metal hosts are rendered more electrophilic. Furthermore, after reflecting on the structures derived from DFT, it seems likely that the two-carbon lariat is insufficient to properly exploit the electrophilic nature of simple cations. Preliminary studies suggest that extending the lariat by one carbon (e.g. a propyl linker) increases the favorability of binding by as much as 5 - 7 kcal/mol. Future studies within this framework will focus on (1) varying crown sizes for smaller cations (e.g. 9-crown-3 and 12-crown-4) and (2) three- and four-carbon lariat lengths.

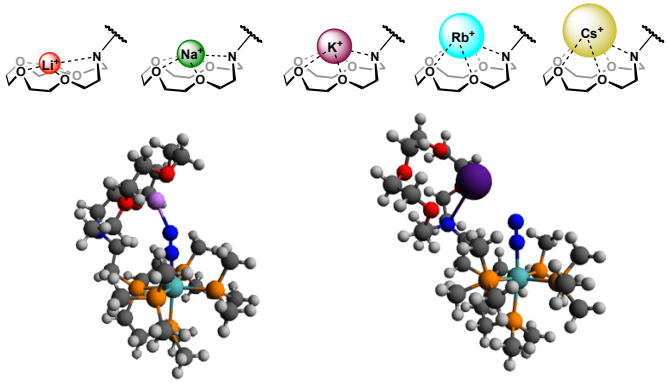

Figure 17. 'Puckering' as a result of binding aza-15-Crown-5 to alkali metals with different sizes (top) and the effect demonstrated in the DFT-derived structures of ***fac*-(15-Crown[M^+]-P_3-Me)$Mo(N_2)(PMe_3)_2$** (M = Li^+ and Cs^+, bottom).

Conclusions

A systematic series of experimental and computational studies have been conducted on alkali metal interactions with dinitrogen ligands in mono- and bis-Mo(N_2) complexes, revealing complex equilibria as a result of the balance between interactions with substrates and solvents. The effects of alkali metal coordination, which lower $\nu(N_2)$ stretching frequencies by 14 – 39 cm^{-1}, where the largest changes in N_2 stretching frequencies were seen with Li^+. Notably, these sorts of shifts in the $\nu(N_2)$ stretching frequencies are of the same order as what might be expected from more significant primary coordination sphere changes (i.e. changes to the phosphine ligand framework) but are induced by readily reversible alkali metal coordination. Although the fact that Li^+ had the strongest effect on the bonding in N_2 was expected on the basis of Fajan's Rules,[87–89] it was surprising that this was offset by a far weaker overall binding affinity. In particular, longer lariat lengths may better position cations to bind and more strongly stabilize N_2 in preparation for chemical functionalization. The ligand frameworks in this report show promise for secondary coordination sphere studies, and efforts are ongoing to further derivatize the ligand framework to improve crystallinity of products and to examine the impacts of lariat length and smaller crown sizes on binding equilibria.

Experimental

All manipulations were conducted under N_2, Ar or using high-vacuum line and glovebox techniques unless otherwise noted. All ambient-pressure chemistry was carried out under a pressure of approximately 590 torr (elevation ~7220 ft) and a temperature of 22±3 ºC unless otherwise stated; a table of pressure-corrected boiling points for the solvents used in this manuscript are reported in Table 13. All solvents were dried using an Innovative Technologies PureSolv Solvent Purification System. Deuterated solvents used in NMR studies were dried over activated 3 Å molecular sieves. NMR spectra were obtained on Bruker DRX-400 or DRX-600 instruments using NMR tubes fitted with re-sealable Teflon valves. ^1H and ^{13}C NMR spectra were referenced internally to either tetramethylsilane or residual protic solvent peaks. ^{31}P NMR spectra were referenced to an 85% H_3PO_4 external standard. Unless otherwise specified, reagents were purchased from Sigma-Aldrich and used without further purification. Infrared spectra were recorded on a PerkinElmer Frontier FT-IR spectrometer in liquid cell composed of quartz. Synthetic, spectroscopic and computational details are available in the Electronic Supplementary Information. The X-ray diffraction data for [*mer*-(18-Crown[H^+]-P_3)$MoCl_3$]$Cl{\cdot}½Et_2O$ and [(18-crown-[H^+]-[$Ca(OTf)_2$]-P_3-Ph)$MoCl_2(PPh_2Me)$]·(1½ toluene) were measured on a Bruker SMART APEX II diffractometer.

a. General synthetic procedure of (n-Crown-P_3-Ph)Mo(N_2) (PMe_3)$_2$

In the glovebox, a 50 mL Schlenk flask was equipped with a magnetic stir bar, 0.21 mmol (n-Crown-Ph)$MoCl_3$ an 9.0 g 0.92 m/m % Na/Hg amalgam (2.83 mmol). The sealed system was taken out from the box and cooled to 0°C under N_2 atmosphere. 16 mg of PMe_3 in 2 mL (0.21 mmol, 8 mg/mL) was added dropwise under vigorous stirring. Another 12 mL THF was injected into the reaction flask and the reaction was running for 1 h at 0°C, then it was stirred for an additional 23 hours at ambient temperature. The flask was pumped into the glovebox, and the suspension was filtered through a 0.45 µm PTFE syringe filter. Solvent was evaporated *in vacuo*, resulting a dark brown crude product. Methanol was added (~15 mL) and the solution was transferred into a separatory funnel, ~15 mL hexane was added and the MeOH phase was extracted eight times. The MeOH phases were combined and solvent was evaporated *in vacuo*. (15-Crown-Ph)$MoN_2(PMe_3)_2$: viscous, brown oil (144 mg, 70%); (18-Crown-Ph)$MoN_2(PMe_3)_2$: viscous, brown oil (166 mg, 77%).

b. General synthetic procedure of (n-Crown-P_3-iPr)Mo(N_2)$_2$ (PPh_2Me)

In the glovebox, a 20 mL glass vial was charged with $Mo(N_2)_2(PPh_2Me)_4$ (200 mg, 0.21 mmol), a magnetic stir bar, n-Crown-iPr (0.21 mmol, 15-Crown-iPr: 119 mg, 18-Crown-iPr: 129 mg) and 5 mL THF. The dark brown solution was stirred for 9 h, followed by concentration *in vacuo*. A glass frit funnel was charged with a silica gel / toluene suspension then the excess toluene was removed by *vacuo*. The crude product in 2-3 mL toluene was layered on the top of the silica and washed with toluene excessively (3 x 20 mL). The solid phase was washed with THF until all the dark brown/yellow material was washed off from the silica pad. THF phases were combined followed by concentration *in vacuo* resulting a dark orange/brown oil. (15-Crown-iPr)$Mo(N_2)_2(PPh_2Me)$: brown/orange thick oil (112 mg, 58 %); (18-Crown-iPr)$Mo(N_2)_2(PPh_2Me)$: brown/orange thick oil (91 mg, 45%).

Conflicts of interest

The authors declare that there are no conflicts of interest.

Acknowledgements

The authors are grateful to Profs. Dean Roddick and Ed Clennan for helpful discussions and for the recent upgrade to Gaussian 16. The authors also gratefully acknowledge financial support from the Wyoming NASA Space Grant Consortium (#NNX15AK56A, Graduate Research Fellowship to L.P.), the Institutional Development Award (IDeA) from the National Institute of General Medical Health Sciences of the National Institutes of Health (Grant # 2P20GM103432, R.A support for L.P. and funding for Oxford Cobra Cryostream 800), the National Science Foundation (CHE-0619920, N.A.; CHE-1358498, REU Program, A.C.; CHE-1147542 and CHE-1762161, Prof. Ed Clennan; CHE-1566622 and CHE-1213903, Prof. Dean Roddick). The project described was also supported by the UW Office of Vice President of Research, UW School of Energy Resources, and the UW Department of Chemistry. The authors thank Kasey Trotter (funded by the Wyoming Research Scholars Program) and Prof. Robert Corcoran for helpful discussions.

References

(1) Tutusaus, O.; Ni, C.; Szymczak, N. K. *J. Am. Chem. Soc.* **2013**, *135* (9), 3403–3406.

(2) Lucas, R. L.; Zart, M. K.; Murkerjee, J.; Sorrell, T. N.; Powell, D. R.; Borovik, A. S. *J. Am. Chem. Soc.* **2006**, *128* (48), 15476–15489.

(3) Liu, T.; DuBois, D. L.; Bullock, R. M. *Nat. Chem.* **2013**, *5* (3), 228–233.

(4) Rakowski DuBois, M.; DuBois, D. L. *Acc. Chem. Res.* **2009**, *42* (12), 1974–1982.

(5) Dubois, D. L. *Inorg. Chem.* **2014**, *53* (8), 3935–3960.

(6) Raugei, S.; Chen, S.; Ho, M.-H.; Ginovska-Pangovska, B.; Rousseau, R. J.; Dupuis, M.; DuBois, D. L.; Bullock, R. M. *Chem. - A Eur. J.* **2012**, *18* (21), 6493–6506.

(7) Barton, B. E.; Olsen, M. T.; Rauchfuss, T. B. *J. Am. Chem. Soc.* **2008**, *130* (50), 16834–16835.

(8) Cowie, B. E.; Emslie, D. J. H. *Chem. - A Eur. J.* **2014**, *20* (51), 16899–16912.

(9) Miller, A. J. M.; Labinger, J. a; Bercaw, J. E. *J. Am. Chem. Soc.* **2008**, *130* (36), 11874–11875.

(10) Barnett, B. R.; Moore, C. E.; Rheingold, A. L.; Figueroa, J. S. *J. Am. Chem. Soc.* **2014**, *136* (29), 10262–10265.

(11) Tseng, K. N. T.; Kampf, J. W.; Szymczak, N. K. *J. Am. Chem. Soc.* **2016**, *138* (33), 10378–10381.

(12) Liu, T.; Wang, X.; Yin, D. *RSC Adv.* **2015**, *5* (92), 75794–75805.

(13) Mao, S. S.; Shen, S.; Guo, L. *Prog. Nat. Sci. Mater. Int.* **2012**, *22* (6), 522–534.

(14) Takeda, H.; Cometto, C.; Ishitani, O.; Robert, M. *ACS Catal.* **2017**, *7* (1), 70–88.

(15) Wang, X.; Shi, H.; Kwak, J. H.; Szanyi, J. *ACS Catal.* **2015**, *5* (11), 6337–6349.

(16) Chantarojsiri, T.; Ziller, J. W.; Yang, J. Y. **2018**, 2567–2574.

(17) Wiedner, E. S.; Roberts, J. A. S.; Dougherty, W. G.; Kassel, W. S.; Dubois, D. L.; Bullock, R. M. *Inorg. Chem.* **2013**, *52* (17), 9975–9988.

(18) DuBois, D. L. *Inorg. Chem.* **1984**, *23* (14), 2047–2052.

(19) Buss, J. A.; Oyala, P. H.; Agapie, T. *Angew. Chemie Int. Ed.* **2017**, *56* (46), 14502–14506.

(20) Tsui, E. Y.; Tran, R.; Yano, J.; Agapie, T. *Nat. Chem.* **2013**, *5*, 293.

(21) Shibasaki, M.; Sasai, H.; Arai, T. *Angew. Chemie Int. Ed. English* **1997**, *36* (12), 1236–1256.

(22) Shu-Kun, L. *Lewis Acids in Organic Synthesis. By Yamamoto, Hisashi*; 2000; Vol. 5.

(23) Jew, S.; Jeong, B.-S.; Lee, J.-H.; Yoo, M.-S.; Lee, Y.-J.; Park, B.; Kim, M. G.; Park, H. *J. Org. Chem.* **2003**, *68* (11), 4514–4516.

(24) Yamaguchi, M.; Shiraishi, T.; Hirama, M. *Angew. Chemie Int. Ed. English* **1993**, *32* (8), 1176–1178.

(25) Nazarov, I.N.; Zaretskaya, I.I. (1941), Izv. Akad. Nauk. SSSR, S. K. 211–224. .

(26) Sai, M.; Matsubara, S. *Synlett* **2014**, *25* (14), 2067–2071.

(27) Larini, P.; Guarna, A.; Occhiato, E. G. *Org. Lett.* **2006**, *8* (4), 781–784.

(28) Grant, T. N.; West, F. G. *J. Am. Chem. Soc.* **2006**, *128* (29), 9348–9349.

(29) Vaidya, T.; Cheng, R.; Carlsen, P. N.; Frontier, A. J.; Eisenberg, R. *Org. Lett.* **2014**, *16* (3), 800–803.

(30) He, W.; Sun, X.; Frontier, A. J. *J. Am. Chem. Soc.* **2003**, *125* (47), 14278–14279.

(31) Zhu, L.; Xi, Z.-G.; Lv, J.; Luo, S. *Org. Lett.* **2013**, *15* (17), 4496–4499.

(32) Kumar, A. *Chem. Rev.* **2001**, *101* (1), 1–19.

(33) Grieco, P. A.; Moher, E. D. *Tetrahedron Lett.* **1993**, *34* (35), 5567–5570.

(34) Jurczak, J.; Gołębiowski, A.; Raczko, J. *Tetrahedron Lett.* **1988**, *29* (46), 5975–5978.

(35) Danishefsky, S.; Kobayashi, S.; Kerwin, J. F. *J. Org. Chem.* **1982**, *47* (10), 1981–1983.

(36) Fujiki, K.; Ikeda, S.; Kobayashi, H.; Mori, A.; Nagira, A.; Nie, J.; Sonoda, T.; Yagupolskii, Y. *Chem. Lett.* **2000**, *29* (1), 62–63.

(37) Ishikawa, T.; Oku, Y.; Kotake, K.-I.; Ishii, H. *J. Org. Chem.* **1996**, *61* (19), 6484–6485.

(38) Bannister, W. H. *Biochem. Educ.* **1992**, *20* (1), 62–63.

(39) Zhou, X.; Kay, S.; Toney, M. D. *Biochemistry* **1998**, *37* (16), 5761–5769.

(40) Speir, J. **2015**, *21* (1), 14–21.

(41) L., M. *J. Orthomol. Med.* **2014**, *29* (3), 101–108.

(42) Toney, M.; Hohenester, E.; Cowan, S.; Jansonius, J. *Science (80-.).* **1993**, *261* (5122), 756–759.

(43) Borovik, A. S. *Chem. Soc. Rev.* **2011**, *40* (4), 1870.

(44) Liu, J.; Choe, J. K.; Wang, Y.; Shapley, J. R.; Werth, C. J.; Strathmann, T. J. *ACS Catal.* **2015**, *5* (2), 511–522.

(45) Ford, C. L.; Park, Y. J.; Matson, E. M.; Gordon, Z.; Fout, A. R. *Science (80-.).* **2016**, *354* (6313), 741–743.

(46) Smil, V. (2000) Cycles of Life, Scientific American Library, N. Y. .

(47) Burgess, B. K.; Lowe, D. J. *Chem. Rev.* **1996**, *96* (7), 2983–3012.

(48) Alberty, R. *Biochemistry*. Washington, DC : 1992, p 10610.

(49) Spatzal, T.; Perez, K. A.; Einsle, O.; Howard, J. B.; Rees, D. C. *Science (80-.).* **2014**, *345* (6204), 1620 LP – 1623.

(50) Dance, I. *Dalt. Trans.* **2012**, *41* (25), 7647–7659.

(51) Igarashi, R. Y.; Laryukhin, M.; Dos Santos, P. C.; Lee, H.-I.; Dean, D. R.; Seefeldt, L. C.; Hoffman, B. M. *J. Am. Chem. Soc.* **2005**, *127* (17), 6231–6241.

(52) Creutz, S. E.; Peters, J. C. *Chem. Sci.* **2017**, *8* (3), 2321–2328.

(53) Geri, J. B.; Shanahan, J. P.; Szymczak, N. K. *J. Am. Chem. Soc.* **2017**, *139* (16), 5952–5956.

(54) Appl, M. *Ullmann's Encyclopedia of Industrial Chemistry*. December 2006.

(55) Burgess, A.; Shah, K.; Hough, O.; Hynynen, K. **2016**, *15* (5), 477–491.

(56) 1951, M. A. G. der A. V. C. .

(57) Grubel, K.; Brennessel, W. W.; Mercado, B. Q.; Holland, P. L. *J. Am. Chem. Soc.* **2014**, *136* (48), 16807–16816.

(58) Allen, A. D.; Senoff, C. V. *Chem. Commun.* **1965**, No. 24, 621.

(59) Broda, H.; Hinrichsen, S.; Tuczek, F. *Coord. Chem. Rev.* **2013**, *257* (2), 587–598.

(60) Hinrichsen, S.; Kindjajev, A.; Adomeit, S.; Krahmer, J.;

Näther, C.; Tuczek, F. *Inorg. Chem.* **2016**, *55* (17), 8712–8722.
(61) Stucke, N.; Flöser, B. M.; Weyrich, T.; Tuczek, F. *Eur. J. Inorg. Chem.* **2018**, *2018* (12), 1337–1355.
(62) Gradert, C.; Stucke, N.; Krahmer, J.; Näther, C.; Tuczek, F. *Chem. - A Eur. J.* **2015**, *21* (3), 1130–1137.
(63) Weiss, C. J.; Groves, A. N.; Mock, M. T.; Dougherty, W. G.; Kassel, W. S.; Helm, M. L.; Dubois, D. L.; Bullock, R. M. *Dalt. Trans.* **2012**, *41* (15), 4517–4529.
(64) Connor, G. P.; Holland, P. L. *Catal. Today* **2017**, *286*, 21–40.
(65) Burford, R. J.; Fryzuk, M. D. *Nat. Rev. Chem.* **2017**, *1*.
(66) Shaver, M. P.; Fryzuk, M. D. *Adv. Synth. Catal.* **2003**, *345* (910), 1061–1076.
(67) Fryzuk, M. D. *Chem. Rec.* **2003**, *3* (1), 2–11.
(68) Galindo, A.; Gutiérrez, E.; Monge, A.; Paneque, M.; Pastor, A.; Pérez, P. J.; Rogers, R. D.; Carmona, E. *J. Chem. Soc. Dalt. Trans.* **1995**, No. 23, 3801–3808.
(69) Ohki, Y.; Aoyagi, K.; Seino, H. *Organometallics* **2015**, *34* (13), 3414–3420.
(70) Gradert, C.; Stucke, N.; Krahmer, J.; Näther, C.; Tuczek, F. *Chem. - A Eur. J.* **2015**, *21* (3), 1130–1137.
(71) Stephan, G. C.; Peters, G.; Lehnert, N.; Habeck, C. M.; Näther, C.; Tuczek, F. *Can. J. Chem.* **2005**, *83* (4), 385–402.
(72) Betley, T. A.; Peters, J. C. *J. Am. Chem. Soc.* **2003**, *125* (36), 10782–10783.
(73) Bonomo, L.; Stern, C.; Solari, E.; Scopelliti, R.; Floriani, C. *Angew. Chemie - Int. Ed.* **2001**, *40* (8), 1449–1452.
(74) Miyazaki, T.; Tanabe, Y.; Yuki, M.; Miyake, Y.; Nakajima, K.; Nishibayashi, Y. *Chem. - A Eur. J.* **2013**, *19* (36), 11874–11877.
(75) Alex Rudd, P.; Planas, N.; Bill, E.; Gagliardi, L.; Lu, C. C. *Eur. J. Inorg. Chem.* **2013**, *2* (22–23), 3898–3906.
(76) Del Castillo, T. J.; Thompson, N. B.; Suess, D. L. M.; Ung, G.; Peters, J. C. *Inorg. Chem.* **2015**, *54* (19), 9256–9262.
(77) Ung, G.; Peters, J. C. *Angew. Chemie - Int. Ed.* **2015**, *54* (2), 532–535.
(78) Ferguson, R.; Solari, E.; Floriani, C.; Chiesi-Villa, A.; Rizzoli, C. *Angew. Chemie Int. Ed. English* **1993**, *32* (3), 396–397.
(79) Fernández, I.; Trovitch, R. J.; Lobkovsky, E.; Chirik, P. J. *Organometallics* **2008**, *27* (1), 109–118.
(80) Fout, A. R.; Basuli, F.; Fan, H.; Tomaszewski, J.; Huffman, J. C.; Baik, M. H.; Mindiola, D. J. *Angew. Chemie - Int. Ed.* **2006**, *45* (20), 3291–3295.
(81) Rittle, J.; Peters, J. C. *J. Am. Chem. Soc.* **2016**, jacs.6b01230.
(82) Scott, J.; Vidyaratne, I.; Korobkov, I.; Gambarotta, S.; Budzelaar, P. H. M. *Inorg. Chem.* **2008**, *47* (3), 896–911.
(83) Semproni, S. P.; Knobloch, D. J.; Milsmann, C.; Chirik, P. J. *Angew. Chemie - Int. Ed.* **2013**, *52* (20), 5372–5376.
(84) Tondreau, A. M.; Milsmann, C.; Patricks, A. D.; Hoyt, H. M.; Lobkovsky, E.; Wieghardt, K.; Chirik, P. J. *J. Am. Chem. Soc.* **2010**, *132* (42), 15046–15049.
(85) Yamamoto, A.; Miura, Y.; Ito, T.; Chen, H. L.; Iri, K.; Ozawa, F.; Miki, K.; Kasai, N.; Sei, T.; Tanaka, N. *Organometallics* **1983**, *2* (10), 1429–1436.
(86) Kieffer, I. A.; Treich, N. R.; Fernandez, J. L.; Heiden, Z. M. *Dalt. Trans.* **2018**.
(87) Fajans, K. *Naturwissenschaften* **1923**, *11* (10), 165–172.
(88) Fajans, K.; Joos, G. *Zeitschrift für Phys.* **1924**, *23* (1), 1–46.
(89) Fajans, K. *Zeitschrift für Krist. - Cryst. Mater.* **1924**, *61* (1–6).
(90) Medford, A. J.; Vojvodic, A.; Hummelshøj, J. S.; Voss, J.; Abild-Pedersen, F.; Studt, F.; Bligaard, T.; Nilsson, A.; Nørskov, J. K. *J. Catal.* **2015**, *328*, 36–42.
(91) McLain, S. J. *J. Am. Chem. Soc.* **1983**, *105*, 6355–6357.
(92) McLain, S. J. *Inorg. Chem.* **1986**, *25* (18), 3124–3127.
(93) Pap, L. G.; Arulsamy, N.; Hulley, E. B. *Polyhedron* **2018**, *141*, 385–392.
(94) Koppe, K.; Bilir, V.; Frohn, H. J.; Mercier, H. P. A.; Schrobilgen, G. J. *Inorg. Chem.* **2007**, *46* (22), 9425–9437.
(95) Parvez, M.; Piers, W. E.; Ghesner, L. *Acta Crystallogr. Sect. E Struct. Reports Online* **2005**, *61* (9), 1801–1803.
(96) Krossing, I.; Reisinger, A. *Coord. Chem. Rev.* **2006**, *250* (21–22), 2721–2744.
(97) Levente G. Pap, Adam Couldridge, Navamoney Arulsamy, E. B. H. *Submitted*.
(98) Bulten, E. J.; van den Hurk, J. W. G. *J. Organomet. Chem.* **1978**, *162* (2), 161–169.
(99) Wieghardt, K.; Hahn, M.; Swiridoff, W.; Weiss, J. *Inorg. Chem.* **1984**, *23* (1), 94–99.
(100) Ning, Y.; Sarjeant, A. A.; Stern, C. L.; Peterson, T. H.; Nguyen, S. T. *Inorg. Chem.* **2012**, *51* (5), 3051–3058.
(101) Steed, J. W. *Coord. Chem. Rev.* **2001**, *215* (1), 171–221.
(102) Grajeda, J.; Kita, M. R.; Gregor, L. C.; White, P. S.; Miller, A. J. M. *Organometallics* **2016**, *35* (3), 306–316.
(103) Gokel, G. W.; Stoddart, J. F. *Crown Ethers and Cryptands*; Monographs in Supramolecular Chemistry; The Royal Society of Chemistry, 1991.
(104) Shannon, R. D. *Acta Crystallogr. Sect. A* **1976**, *32* (5), 751–767.
(105) Weigend, F. *Phys. Chem. Chem. Phys.* **2006**, *8* (9), 1057.
(106) Laury, M. L.; Wilson, A. K. *J. Chem. Theory Comput.* **2013**, *9* (9), 3939–3946.
(107) Stark, P. C.; Huff, M.; Babaian, E. A.; Barden, L. M.; Hrncir, D. C.; Bott, S. G.; Atwood, J. L. *J. Incl. Phenom.* **1987**, *5* (6), 683–688.
(108) LeBlanc, F. A.; Decken, A.; Cameron, T. S.; Passmore, J.; Rautiainen, J. M.; Whidden, T. K. *Inorg. Chem.* **2017**, *56* (2), 974–983.
(109) Ichihashi, K.; Konno, D.; Date, T.; Nishimura, T.; Maryunina, K. Y.; Inoue, K.; Nakaya, T.; Toyoda, K.; Tatewaki, Y.; Akutagawa, T.; et al. *Chem. Mater.* **2018**, *30* (20), 7130–7137.
(110) Han, B.; Lu, J.; Kochi, J. K. *Cryst. Growth Des.* **2008**, *8* (4), 1327–1334.
(111) Kather, R.; Lork, E.; Vogt, M.; Beckmann, J. *Zeitschrift für Anorg. und Allg. Chemie* **2017**, *643* (10), 636–641.
(112) Flaig, K. S.; Raible, B.; Mormul, V.; Denninger, N.; Maichle-Mössmer, C.; Kunz, D. *Organometallics* **2018**, *37* (8), 1291–1303.
(113) Liddle, S. T.; Clegg, W. *Polyhedron* **2002**, *21* (23), 2451–2455.
(114) Liddle, S. T.; Clegg, W.; Morrison, C. A. *Dalt. Trans.* **2004**, No. 16, 2514.
(115) Heldt, I.; Behrens, U. *Zeitschrift für Anorg. und Allg. Chemie*

2005, *631* (4), 749–758.

(116) Nurtaeva, A. K.; Holt, E. M. *Acta Crystallogr. Sect. C Cryst. Struct. Commun.* **1998**, *54* (5), 594–597.

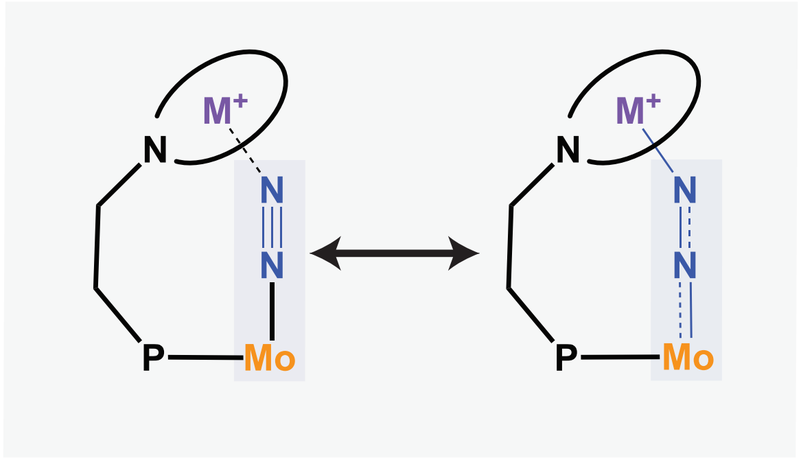
M+
N
N
N
P
Mo
M+
N
N
N
P
Mo

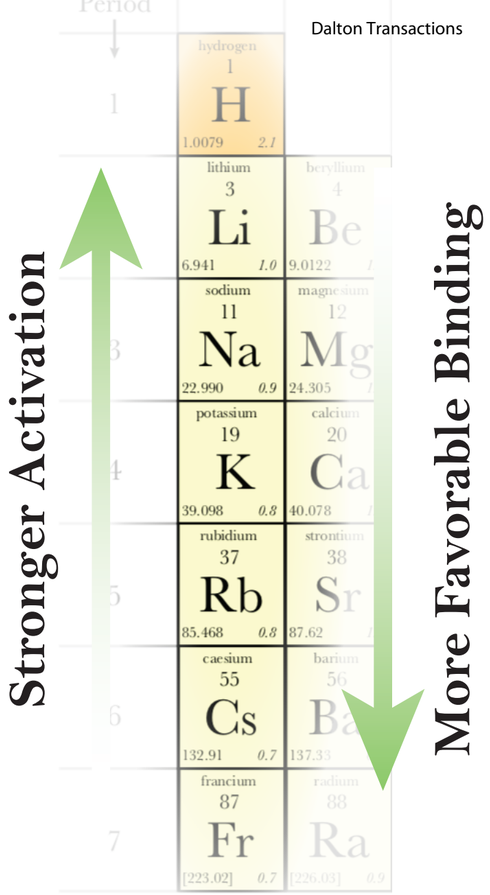
Stronger Activation
More Favorable Binding
hydrogen 1 H 1.0079 2.1
lithium 3 Li 6.941 1.0
beryllium 4 Be 9.0122
sodium 11 Na 22.990 0.9
magnesium 12 Mg 24.305
potassium 19 K 39.098 0.8
calcium 20 Ca 40.078
rubidium 37 Rb 85.468 0.8
strontium 38 Sr 87.62
caesium 55 Cs 132.91 0.7
barium 56 Ba 137.33
francium 87 Fr [223.02] 0.7
radium 88 Ra [226.03] 0.9

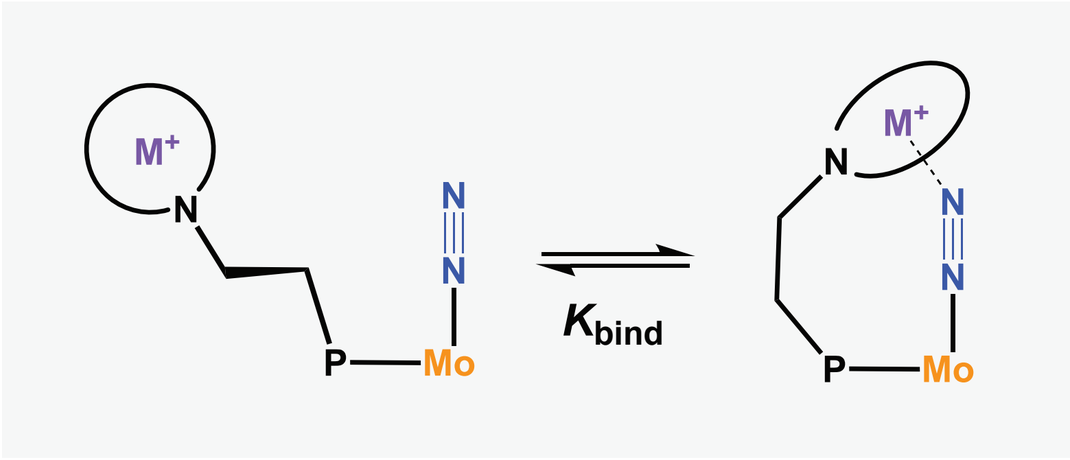
M+
N
N
N
P
Mo
Kbind
M+
N
N
N
P
Mo